Examination of Integrated Velocity Model of Shallow and Deep Structure in Fujisawa City in Japan

S. Senna
National Research Institute for Earth Science and Disaster Prevention, Japan

Y. Inagaki & H. Matsuyama
Oyo Corp, Japan

H. Fujiwara
National Research Institute for Earth Science and Disaster Prevention, Japan

SUMMARY:

In this study, a detailed subsurface structure with about 50m intervals, was obtained based on microtremor measurements and micro-gravity measurements carried on in the whole area of Fujisawa city. An initial ground structural model was made by borehole data offered from the Fujisawa city. The reverse-analysis by the H/V spectral ratio and the phase velocity was applied on the initial model. A final structural model was made from statistic averaging the individual S wave velocity at the same geological layer. The spectral amplification rate obtained from our model is consistent with that of earthquake ground motion recorded by the K-NET Fujisawa station.

Keywords: Velocity structure model, Microtremor survey, H/V spectrum, Gravity survey, Borehole data

1. INTRODUCTION

We conducted microtremor observations throughout Fujisawa City, to construct a detailed soil-structure model. To use the soil-structure model as the basis for analysis, we adopted the existing deep-soil-structure model for regions deeper than engineering bedrock, and created a shallow geological structure model from the geologic columns provided by Fujisawa City or collected by ourselves. In the initial stage, we combined the two models to form a shallow-and-deep integrated ground model. To create a velocity–structure model, we processed the above-mentioned initial ground model, the phase velocity of the microtremor search results, and microtremor observation results at a single point (H/V spectral ratio) by joint inversion, the calculated the average S-wave speed for each geological strata, and modified the shallow-and-deep integrated ground model. The important result of this study, we constructed a model of buried valleys left unexplained by the geological model using gravity measurements conducted.

2. SUMMARY OF MIMICROTREMOR OBSERBATION

We conducted microtremor observations in March 2010, mainly in the municipal facilities and premises of Fujisawa City. We selected 436 locations such as municipal elementary- and junior high schools, municipal facilities, and parks, to provide measurements at intervals of approximately 500 m. As the geological literature indicates the existence of buried valleys in the southern part of Fujisawa City (mostly indicated as sand and gravel banks in the geomorphological classifications), measurements in that area were conducted at intervals of approximately 100 m. On the other hand, we selected some municipal elementary and junior high schools to set 16 observation points at intervals of approximately 2,000 m. For the microtremor observations, we used an integrated microtremor observation unit (JU-210, 215, Hakusan Corp.), equipped with two horizontal elements, one vertical element, and a data-logger (LS-7000XT). We conducted microtremor observations at each point for at least 15 minutes. For microtremor array observations, we set up arrays with radii of 40, 20, and 10 m

in most recording locations, and conducted measurement for 40 minutes. Figure 1 shows the observation points for microtremor and array data.

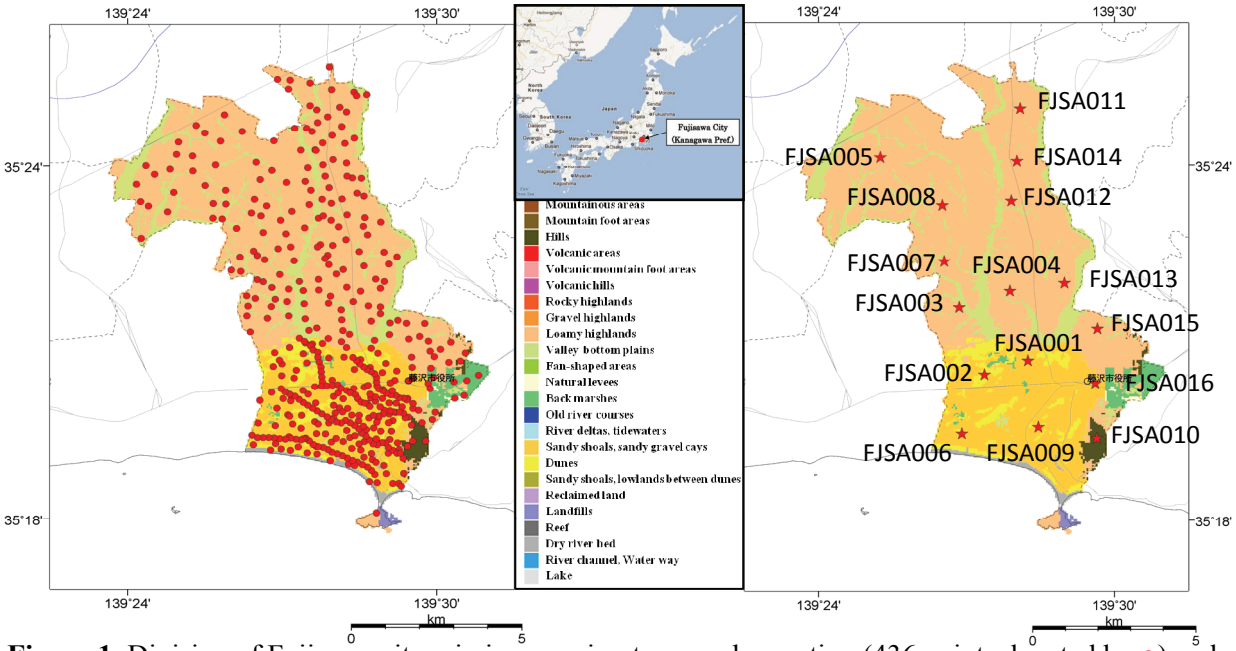

Figure 1. Division of Fujisawa city in japan; microtremor observation (436 points denoted by ●) and array observation (16 points denoted by ★) points

3. CREATION OF INITIAL GROUND MODEL AND CONSTRACTION OF VELOCITY STRUCTURE MODEL

3.1 Collection of Borehole Data and Creation of Initial Ground Model

We used data from 3,231 borehole sites, provided by Fujisawa City and Kanagawa Prefecture to create a shallow-soil-structure model as the initial ground model for this research. The left chart of Figure 2 shows the borehole locations, which cover the entire area of Fujisawa City, but are concentrated in the area from the Fujisawa station of Japan Railways to the Fujisawa Municipal Office. We used an existing soil-structure model of the regions deeper than engineering bedrock. The right chart of Figure 2 shows the initial shallow-and-deep integrated geological model with mesh size of 50 m, that combines the existing deep-soil-structure model with the created shallow-soil-structure model.

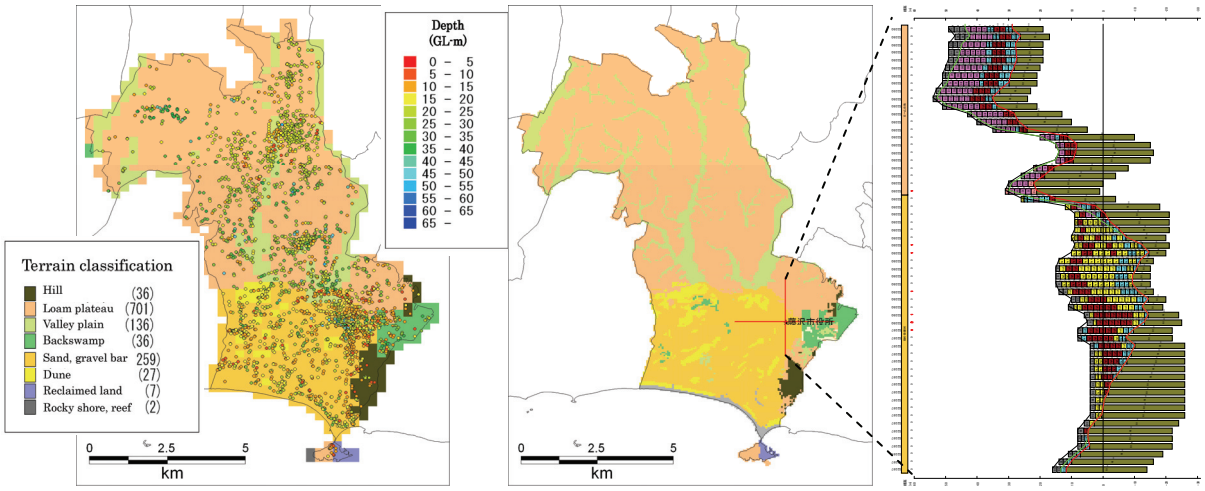

Figure 2. Boundary of the created shallow-ground soil-structure model and the distribution of borehole data (left chart); the process of creating 50m-mesh shallow-and-deep integrated ground-model of Fujisawa City (right chart)

Based on the stratigraphy classification at the borehole sites, we organized the trend of depth distribution of N values in each stratum, and set a representative value for each stratigraphy classification. Subsequently, we converted the shallow and deep integrated model to a velocity–structure model by converting the N values into S-wave velocity values. Using the same method, we established a representative density value from the N values. Table 1 shows the relationship between S-wave velocity and N value.

Table 1. Relationship between S-wave velocity and N(SPT) value

	Regression of the current data	Regression formula of Central Disaster Prevention Council (Reference)
Cohesive soil (alluvial and diluvial)	$Vs = 123.8 \cdot N^{0.2641}$	$Vs = 111.3 \cdot N^{0.3144}$
Sandy soil (alluvial and diluvial)	$Vs = 90.58 \cdot N^{0.3219}$	$Vs = 94.38 \cdot N^{0.3020}$
Rudaceous soil (alluvial and diluvial)	$Vs = 121.9 \cdot N^{0.2635}$	$Vs = 123.05 \cdot N^{0.2433}$

Table 2. Geological stratum classification, N value, and Vs Velocity of the initial ground model

Stratum No.	Facies and stratigraphy classification	Geological age	Stratigraphy classification		Average N value	initial model Vs(m/s)
1	B(Land surface)	Quaternary Holocene	Surface soil, filling soil		8.5	214
2	E(pt-500)		Peat stratum aggraded on the concaved land surface		1.9	147
3	F(dt-600)		Talus accumulation		17.0	257
4	G(cl-800)		River deposit mainly comprising cohesive soil		6.1	200
5	H(ss-1000)		River deposit mainly comprising sandy soil		14.2	213
6	I(bss-1200)		Deposit of dune and beach ridge		37.1	290
7	J(cl-1300)		Cohesive soil stratum		12.9	243
8	K(SGss-gvl-1400)		River deposit mainly comprising cohesive soil		73.5	378
9	L(cl-1500)		Cohesive soil stratum		8.7	219
10	M(cl-2000)		Marine cohesive sand stratum (Buried valley)		8.6	219
11	ss-5000		Sandy soil		45.1	309
12	cl-5500		Cohesive soil		7.3	209
13	SGss-gvl-7000		Base gravel stratum		106.9	417
14	Lm-10000	Quaternary Pleistocene	Loam and volcanic ash property stratum		7.4	210
15	cl-11000		Volcanic ash property cohesive soil		12.7	242
16	tr-12000		Terrace gravel stratum (Sagamino gavel stratum)		131.7	441
17	cl-18000		Sagami group (Fujisawa silt stratum)	Cohesive soil	24.5	288
18	ss-gvl-20000			Sandy soil, gravel soil	68.2	371
19	cl-30000			Cohesive soil	32.0	309
20	gvl-ss-40000			Sandy soil, gravel soil	166.7	469
21	cl-50000			Cohesive soil	44.4	337
22	ss-hard-60000			Sandy soil, gravel soil	103.0	413
23	cl-65000			Cohesive soil	57.7	361
24	gvl-70000			Sandy soil, gravel soil	74.8	380
25	R-90000	Pre-Pleistocene	Base (Less than Naganuma stratum), weathered part		67.1	369
26	R-100000		Base (Less than Naganuma stratum), unweathered		119.7	430

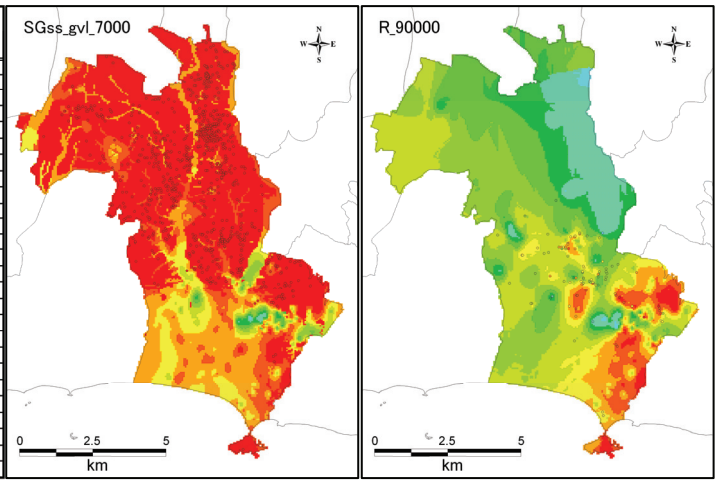

Figure 3. Spatial distribution of lower end depth by geological stratigraphy classification (Left chart: Quaternary Holocene, base gravel stratum; Right chart: Quaternary Pleistocene, Group of Sagami strata gravel stratum)

3.2 Modification of Initial Geological Structure Model by Gravity Measurement

3.2.1 Gravity Measurement and Bouguer Anomaly Charts

We conducted gravity measurement at the black points (4 lateral lines and discrete points) within Fujisawa City, the observed Bouguer anomaly values are shown in Figure 4.1 to 4.3.

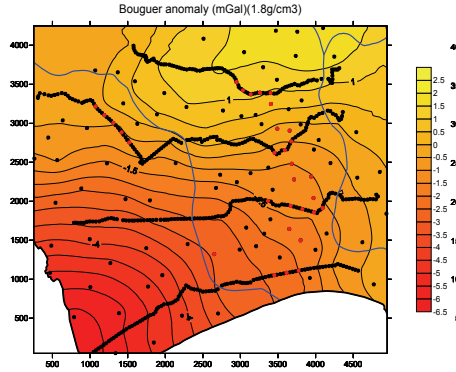

Figure 4.1. Distribution of Bouguer Anomaly.(Density=1.8g/cm^3, Grid interval:50m)

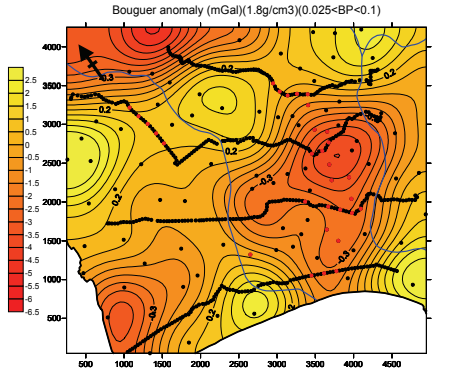

Figure 4.2 Distribution of Bouguer anomaly(D=1.8g/cm^3,Grid int:50m) <long wavelength>

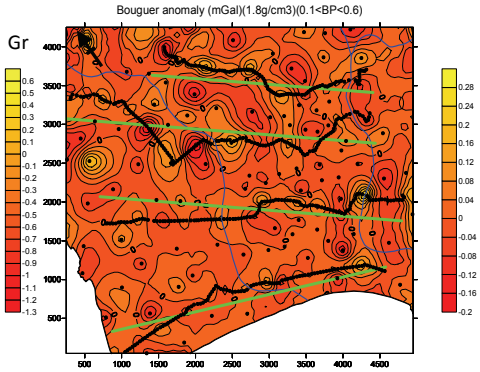

Figure 4.3 Distribution of Bouguer anomaly(D=1.8g/cm^3, Grid int:50m) < short wavelength>

3.2.2 Distribution of Gravity Anomalies, Calculated from the 50m-mesh Geological Stratigraphy of Fujisawa City

We calculated the theoretical gravity values from the 50m-mesh geological stratigraphy of Fujisawa City, using a three-dimensional prism model. Figure 5 and Table 3 show examples of the three-dimensional prism model. The prism shown in red in Fig. 5.1 has the minimum value = X(i) and the maximum value = X(i+1) on the X-axis; and the minimum value = Y(j) and the maximum value = Y(j+1) on the Y-axis. The Z-axis has a surface defined by the following formulae:

Maximum value = (Z(i,j,k)+Z(i+1,j,k)+Z(i,j+1,k),+Z(i+1,j+1,k))/4 (3.1)
Minimum value = (Z(i,j,k+1)+Z(i+1,j,k+1),+Z(i,j+1,k+1)+Z(i+1,j+1,k+1))/4 (3.2)

Here, k is the input number of the boundary surface. For input values beyond the range of the maximum and minimum input values on the X and Y axes, a semi-infinite prism is created automatically, which has a value on the Z-axis at the maximum value (minimum value) (See Table 3).

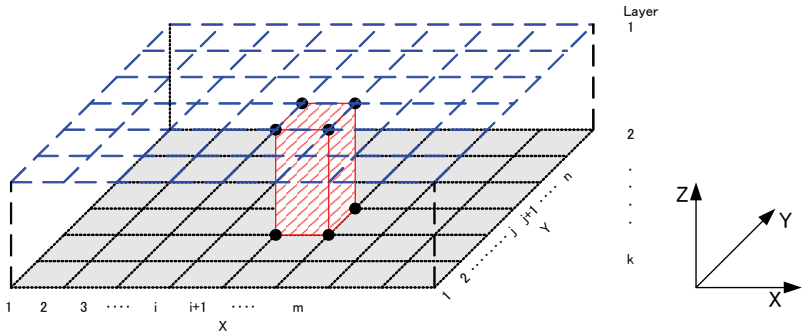

Figure 5. Example of three-dimensional prism

Table 3. Example of three-dimensional prism

Xmin	Xmax	Ymin	Ymax	Zmin	Zmax
X(i)	X(i+1)	Y(j)	Y(j+1)	(Z(i,j,k+1)+Z(i+1,j,k+1)+ Z(i,j+1,k+1)+Z(i+1,j+1,k+1))/4	(Z(i,j,k)+Z(i+1,j,k)+ Z(i,j+1,k)+Z(i+1,j+1,k))/4
-1E07	X(1)	Y(j)	Y(j+1)	(Z(1,j,k+1)+Z(1,j+1,k+1))/2	(Z(1,j,k)+Z(1,j+1,k))/2
X(m)	1E07	Y(j)	Y(j+1)	(Z(m,j,k+1)+Z(m,j+1,k+1))/2	(Z(m,j,k)+Z(m,j+1,k))/2

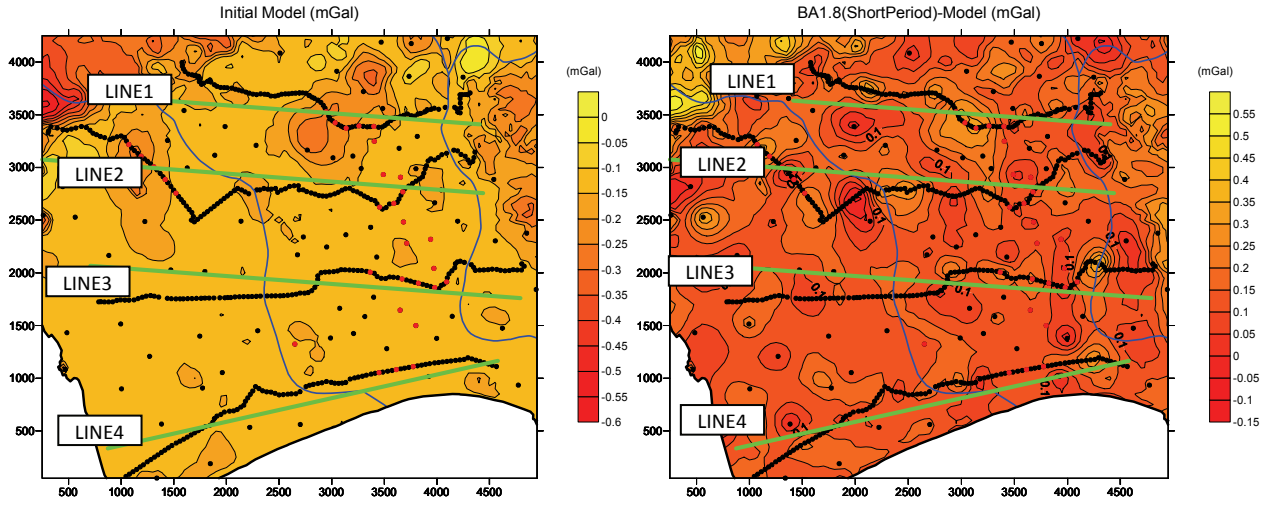

Figure 6. Difference between Bouguer anomaly and gravity anomaly calculated by the model (Density = 1.8g/cm^3, Grid interval: 50 m) <Short-wavelength component>

3.2.3 Estimation of the Depth of a Buried Valley on the Two-Dimensional Cross Section

Figure 7.1 shows the geography near the survey area, Figure 7.2 indicates the outline of the soil structure, and Table 5 gives the stratigraphy classification based on the borehole data. A terrace surface, extending from the plateau, was identified beneath the survey area (coastal lowland). The buried geographical surface is a “wave-cut shelf” in the left (east) bank of the Sagami River, located at a depth of less than 20m, beneath a large area of the coastal lowland(Figure 7.2). As bottom erosion by rivers during the glacial period extended far deeper than the surface of the wave-cut shelf, the eroded river valleys are presumed to have extended to the ocean area as a buried valley, beneath the coastal lowland. During the glacial period, rivers (Hikiji and Sakai Rivers) possibly formed a buried valley in the area of Fujisawa City, and the gravity anomaly near the watershed is assumed to be the buried valley (Figure 7.1). The stratum underlying the buried valley is assumed to be the cl-2000 stratum, according to the stratigraphy classification of the borehole data. This was confirmed by part of the deep borehole data near the lateral survey Line 1, and is reflected in the initial model. However, The continuity of a buried valley cannot be checked only with borehole data collected this time.

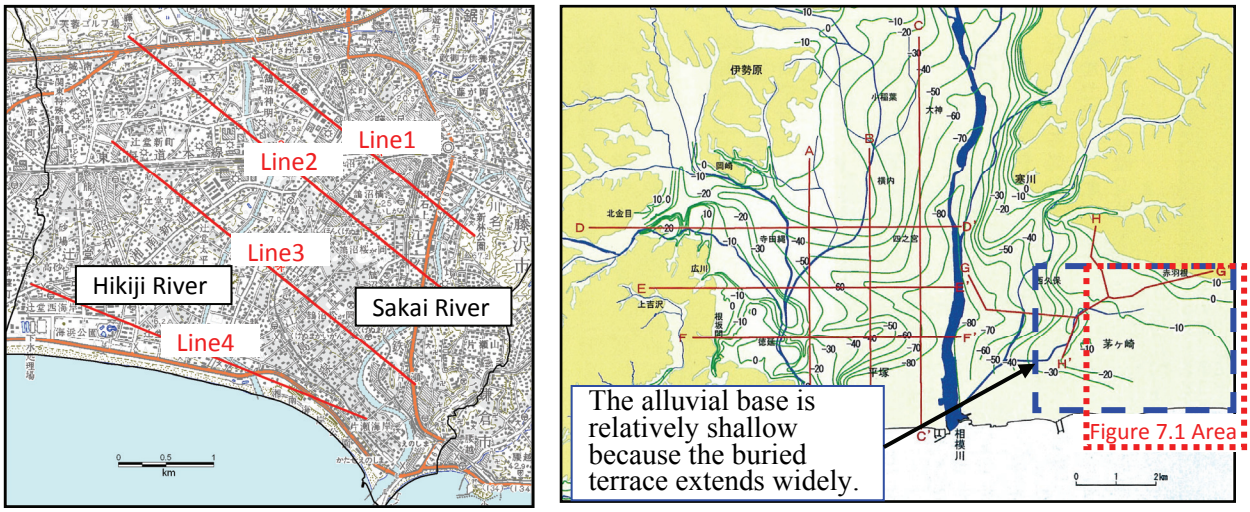

Figure 7.1 Terrain of Fujisawa City and approximatelocation of survey line of gravity observation

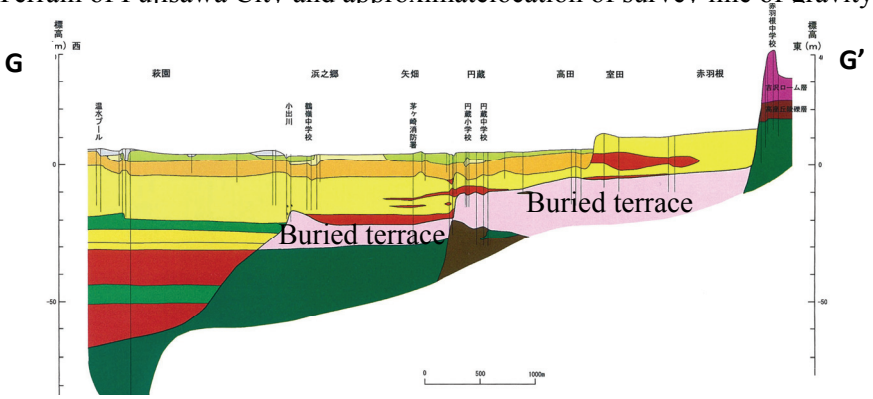

Figure 7.2 Overview of the geological structure of Chigasaki and Fujisawa City

3.2.4 Calculation Method and Results

We repeated the calculation on the assumption that the variation between the gravity anomaly in the initial model and that calculated from the gravity measurement represent the strata underlying the buried valley (cl-2000). Figure 8 shows the calculation flow for the method used. As the initial model, we created two kinds of models. One model segmentalizes the strata within the same stratigraphy (segmentalized model that considers the velocity increase in depth direction in the stratigraphy), and the other model categorizes all deposition layers with internally consistent characteristics as comprising one stratum (one stratum model). All buried valleys were located directly above the basement stratum, the stratum thickness used in one repetitive calculation was set as $\Delta H = 0.1$m, and the density was assumed to be 1.6g/cm^3 (stratum equivalent of Ac3).

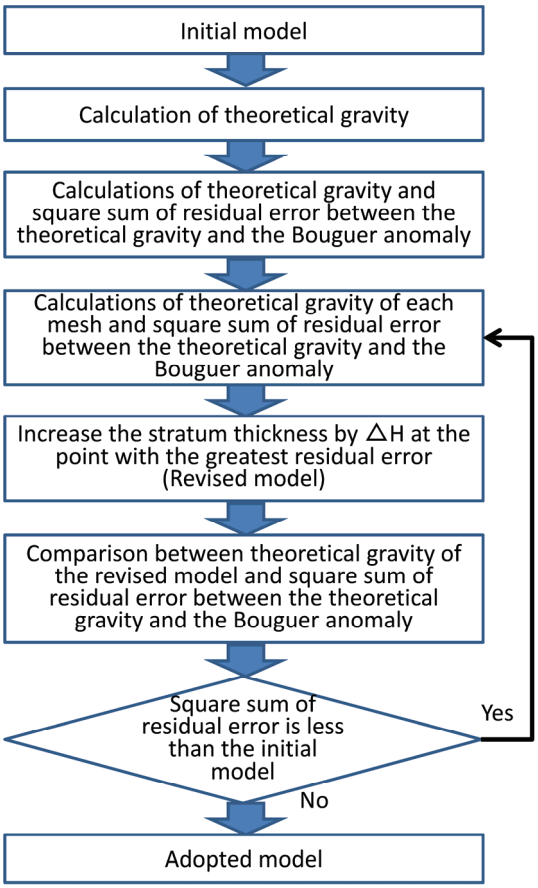

Figure 8. Flow of the iterative

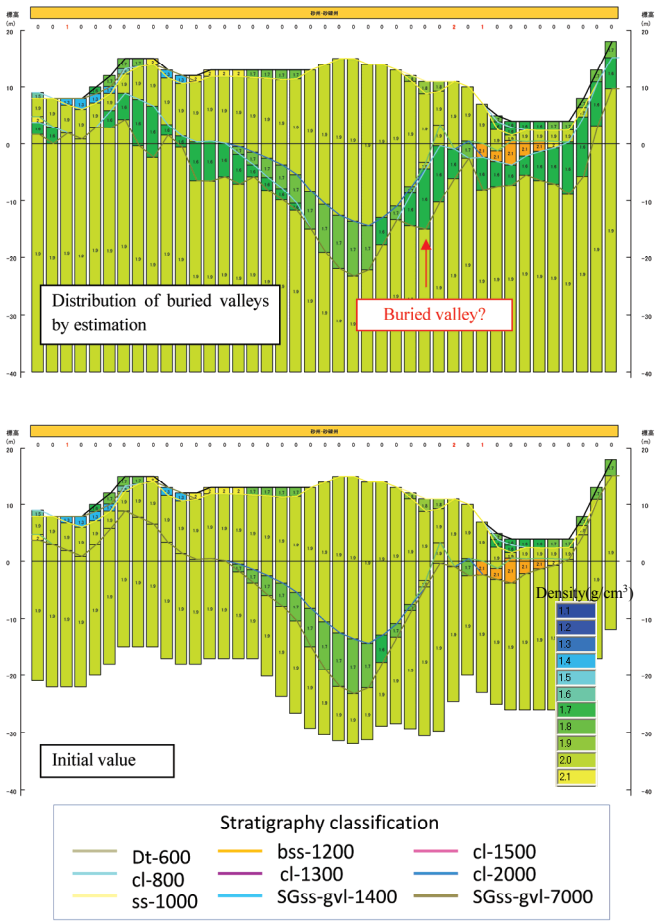

Figure 9. Estimation of stratum underlying the buried valley(Left:Density distribution by the initial model. Right:Density distribution by the final model) (Segmentalized model, Survey Line 1, Buried valley Ac3,ρ = 1.6g/cm3).

Figure 9 show the ground models based on the calculation results. The following points summarize the calculation results. A stratum with aggraded buried valley (hereafter referred to as stratum underlying buried valley), with a width of 4-5 mesh-cells (200-250 m), occurs in the east part of the city in all survey lines. This trend is conspicuous in survey lines 3 and 4, and the depth extends to approximately 15 m. A stratum 3-4 mesh-cells (150-200 m) wide occurs in the west part of the city, although the trend is not as distinct as in the east part of the city. The depth is approximately 5-10 m in survey lines 3 and 4. The same area is visible in survey line 2, at depths greater than 20 m. However, within this range, data are somewhat unreliable because, compared with other ranges, the location of the survey line assumed in the calculation is located far from where gravity was measured.

In survey line 1, the cl-2000 stratum is distributed in the initial model. However, the real Bouguer anomaly is further east than the distribution of the cl-2000 stratum. The cl-2000 stratum in the initial model adopted the stratum structure of the borehole data over short distances, because no existing borehole data are available on this survey line. However, the borehole data possibly correspond to the buried valley. Taking the above analysis into consideration, we conclude that the results indicate the distribution of buried valleys by gravity measurement on the east side of the city. It is possible that the results also indicate the distribution of buried valleys on the west side of the city.

3.2.5 Estimation of the Depth of the Buried Valley on Three-Dimensional Cross Sections

Using the same method as in section 3, we calculated how many low-density strata should be added deeper than the base to explain all of the variations between the Bouguer anomaly and gravity anomaly calculated by the model for the three-dimensional cross sections, assuming that the density is equivalent to Ac3 (1.6g/cm^3). Figure 10.1 shows the low end depth of the base of the initial model;

and Figure 10.2 gives the calculated stratum thickness of the buried valley, respectively. The red lines in Figure 10.2 indicate the locations of the buried valleys, envisaged by the two-dimensional cross section.

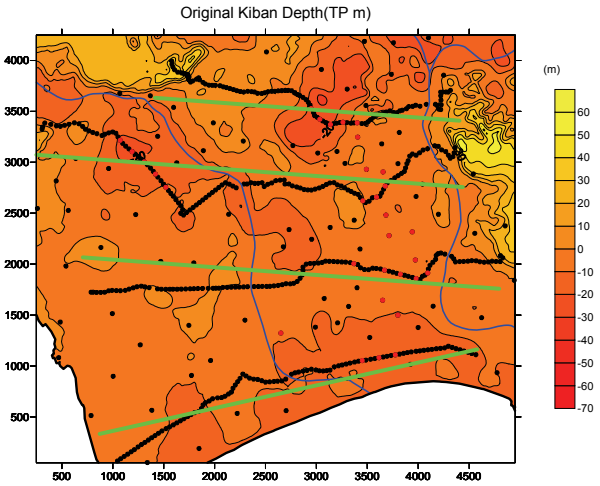

Figure 10.1 Low end depth of the base of the initial

— : The red lines indicate the locations of buried valleys, envisaged by the two-dimensional calculation.

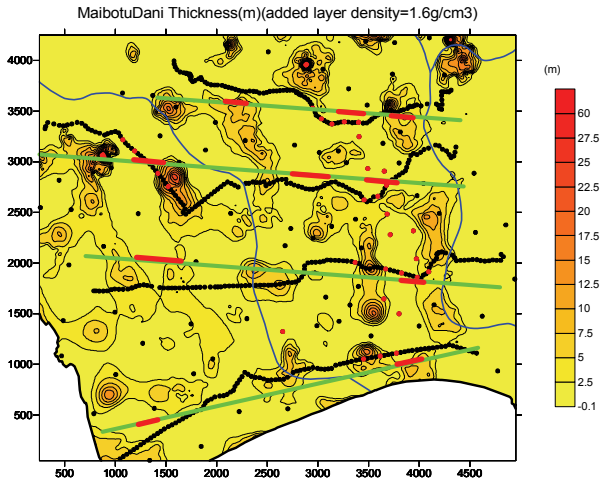

Figure 10.2 Stratum thickness of the buried valley assumed by Bouguer anomaly data.(The density of the buried valley was assumed to be 1.6g/cm^3, and the grid interval is 50 m)

3.3 Modification of the Ground Model Using Analysis of Microtremor Data

Using the shallow-and-deep integrated ground model created in 3.2, we conducted inverse analysis with reference to the method of Arai and Tokimatsu (2004, 2005). In the inverse analysis, we allowed the parameter Vs velocity to fluctuate from the initial value to Vs = 500(m/s), and the stratum thickness to fluctuate by up to 30% in the area of the velocity stratum of the engineering base (Vs = 500, 700 m/s). Figure 11 shows the concept of the inverse analysis of the shallow-and-deep integrated ground model with regard to these analysis conditions. The analysis considered the Rayleigh wave from the base mode to the 4th mode. The evaluation function (denoted by F) that is to be minimized as the convergence criterion was calculated by assigning a weight to the vicinity of the peak observed H/V spectral ratio in the cycle between 0.2 and 2.0s. In this calculation, the junction of the shallow-and-deep integrated and the earthquake intensity, which is calculated as the final criterion, are taken into consideration. Equation (3.3) shows the evaluation function F, the convergence criteria for F, and the conditions indicating that convergence was achieved.

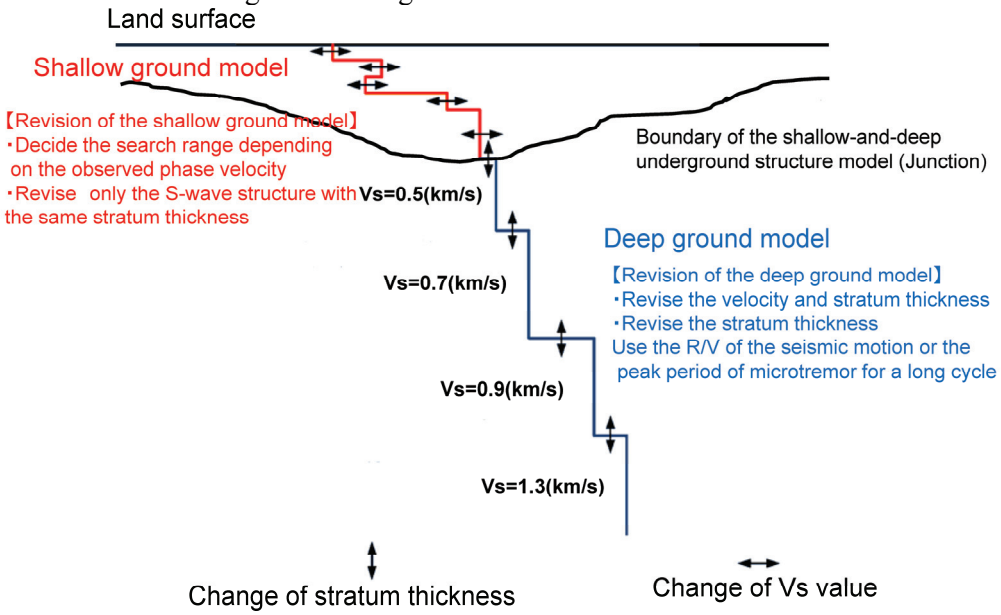

Figure 11. Conceptual diagram of inverse analysis of the shallow-and-deep integrated ground model

$$F = \frac{w_R}{I_R}\sum_{i=1}^{I_R}\left(\frac{c_{mi}^R - c_{Si}^R}{c_{mi}^R}\right)^2 + \frac{w_{HV}}{I_{HV}}\sum_{i=1}^{I_{HV}}\left(\frac{(H/V)_{mi} - (H/V)_{Si}}{(H/V)_{mi}}\right)^2 \quad \text{(Phase velocity and H/V)}$$

$$F = \frac{1}{I_{HV}}\sum_{i=1}^{I_{HV}}\left(\frac{(H/V)_{mi} - (H/V)_{Si}}{(H/V)_{mi}}\right)^2 \quad \text{(H/V only)} \qquad w_R = 1.0\,,\ w_L = 1.0,\ w_{HV} = 1.0 \tag{3.3}$$

Here, c_R, (H/V) is the phase velocity of Rayleigh and surface waves, and each of I_R, I_{HV} refer to the number of data. The suffixes m and S indicate the observed value and theoretical value, respectively. w shows weight, which was set to $w_R = 1.0$, $w_{HV} = 1.0$. In the analysis cycle boundary T, the judgment of convergence of the average residual rate (square root of the evaluation function F) in the iteration is set as the minimum value of the residual. The ratio of Rayleigh wave to Love wave (R/L ratio) was set to a constant of 0.7 in the target cycle, with reference to Tokimatsu and Arai (1998). Using the above conditions, we analyzed joint inversion of H/V spectrum and the phase velocity of microtremor array, using the previously-developed geological model. From the results, we calculated the average velocity Vs of each geological facies, and created a ground model that covers from the stratum equivalent to seismic bedrock to the land surface. Figure 12 compares the theoretical H/V spectral ratio after the joint inversion with the microtremor array observations at 7 elementary- and junior high schools. The phase velocities observed for the microtremors agreed well with the theoretical value in Chogo Elementary School, Shonandai Elementary School, and Takinosawa Junior High School, located in the north and central parts of the city. However, the phase velocity tended to become lower than the phase velocity of the existing ground model between 0.5 and 0.2s, in Meiji Junior High School and Takahara Junior High School, located in the south part of the city. From the resulting H/V spectral ratios, the predominant period varies greatly between the theoretical and observed values. Due to the size of the array radius, we were able to calculate the phase velocity of the current microtremor observation only in the case that the dispersion curve could be obtained in a cycle shorter than 0.7s. We therefore synthesized the phase velocity to prevent large variations, using the theoretical phase velocity by the initial ground model, and used this for the inverse calculation.

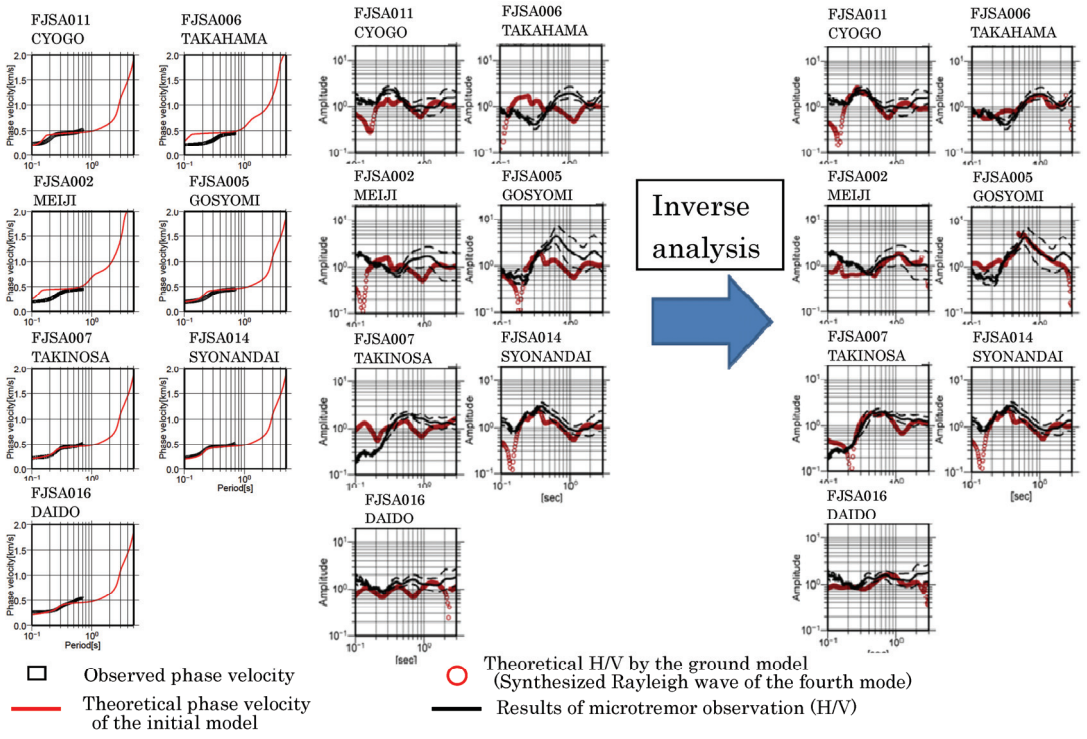

Figure 12. Example of analysis (Left chart: Comparison between the phase velocity of microtremor array (theoretical phase velocity is the Rayleigh wave base), results of the initial ground model, and observation results. Right chart: Comparison between the ground model and microtremor observation results after inversion using the H/V spectral ratio and phase velocity)

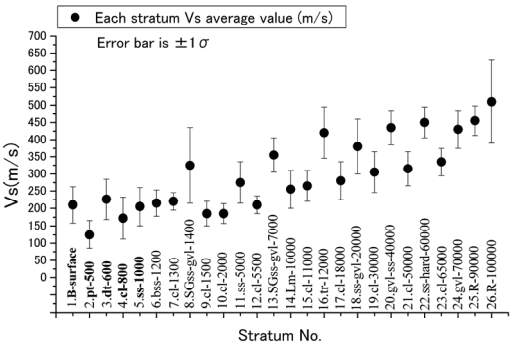

Figure 13. Average and variance calculated for each stratum (Summation in the case of cl-2000 and buried valley)

Table 4. Comparison between initial ground model and analysis

Stratum No.	Facies and stratigraphy classification	Geological age	Stratigraphy classification	Average N value	initial model Vs(m/s)	This study Vs(m/s)	Change rate (This study/initial
1	D(Land surface)	Quaternary Holocene	Surface soil, filling soil	8.5	214	210	0.98
2	E(pt-500)		Peat stratum aggraded on the concaved land surface	1.9	147	135	0.92
3	F(dt-600)		Talus accumulation	17.0	257	235	0.91
4	G(cl-800)		River deposit mainly comprising cohesive soil	6.1	200	180	0.90
5	H(ss-1000)		River deposit mainly comprising sandy soil	14.2	213	210	0.99
6	I(bss-1200)		Deposit of dune and beach ridge	37.1	290	230	0.79
7	J(cl-1300)		Cohesive soil stratum	12.9	243	205	0.84
8	K(SGss-gvl-1400)		River deposit mainly comprising cohesive soil	73.5	378	320	0.85
9	L(cl-1500)		Cohesive soil stratum	8.7	219	190	0.87
10	M(cl-2000)		Marine cohesive sand stratum(Buried valley)	8.6	219	190	0.87
11	MA(Buried valley)						
12	ss-5000		Sandy soil	45.1	309	285	0.92
13	cl-5500		Cohesive soil	7.3	209	210	1.00
14	SGss-gvl-7000		Base gravel stratum	106.9	417	360	0.86
15	Lm-10000	Quaternary Pleistocene	Loam and volcanic ash property stratum	7.4	210	255	1.21
16	cl-11000		Volcanic ash property cohesive soil	12.7	242	265	1.10
17	tr-12000		Terrace gravel stratum (Sagamino gavel stratum)	131.7	441	420	0.95
18	cl-18000		Sagami group (Fujisawa silt stratum) Cohesive soil	24.5	288	280	0.97
19	ss-gvl-20000		Sandy soil, gravel soil	68.2	371	380	1.02
20	cl-30000		Cohesive soil	32.0	309	305	0.99
21	gvl-ss-40000		Sandy soil, gravel soil	166.7	469	435	0.93
22	cl-50000		Cohesive soil	44.4	337	315	0.93
23	ss-hard-60000		Sandy soil, gravel soil	103.0	413	450	1.09
24	cl-65000		Cohesive soil	57.7	361	335	0.93
25	gvl-70000		Sandy soil, gravel soil	74.8	380	430	1.13
26	R-90000	Pre-Pleistocene	Base (Less than Naganuma stratum), weathered part	67.1	369	455	1.23
27	R-100000		Base (Less than Naganuma stratum), unweathered part	119.7	430	495	1.15

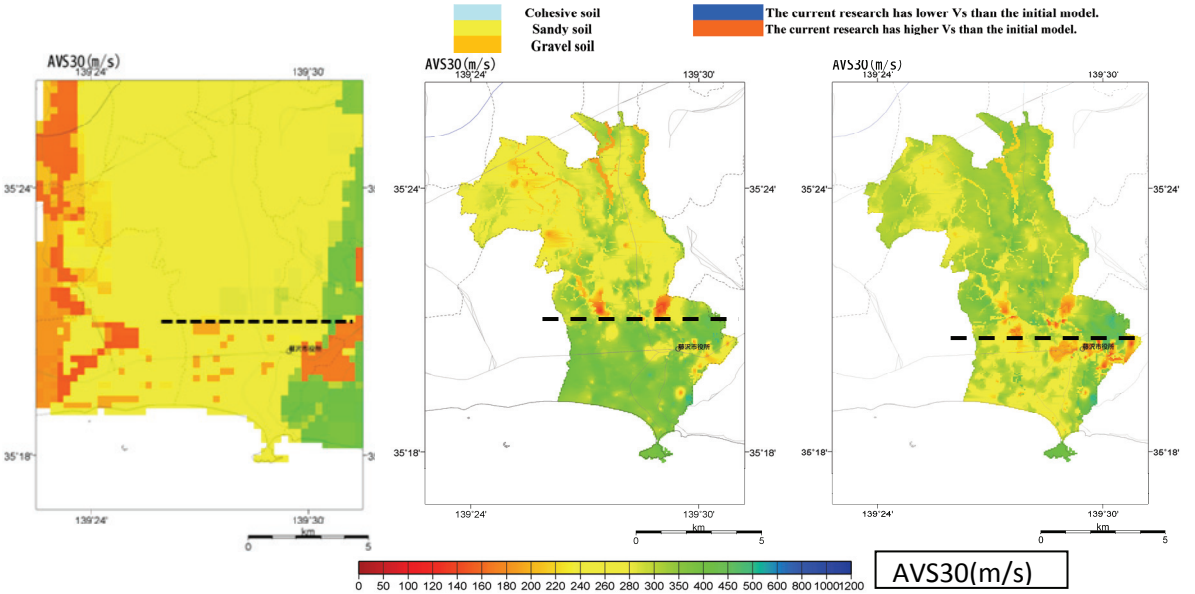

Figure 14. Comparison between the average velocity AVS30. Left chart : Geomorphologic classification(250m mesh). Middle chart : Initial ground model (50m mesh). Right chart : Analysis ground model (50m mesh). Black lines in the figure show the approximate boundary location between alluvial lowland and diluvial plateau

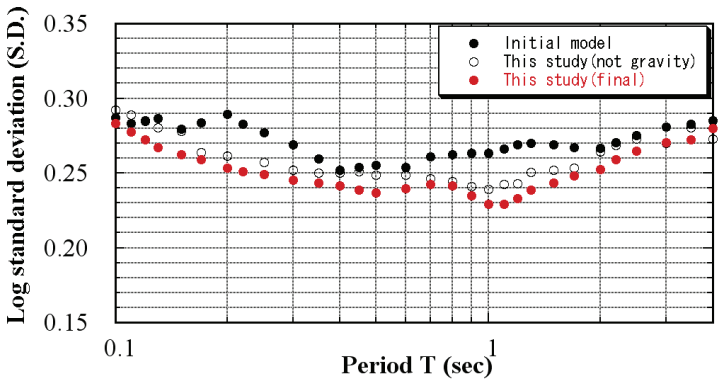

Figure 15. (●) shows the synthesis of microtremor H/V spectralratio in the initial geological modal ; (○) indicates the theoretical H/V spectral ratio of the review ground model and (●) indicates theoretical H/V spectral ratio of the review ground model (with gravity compensation)

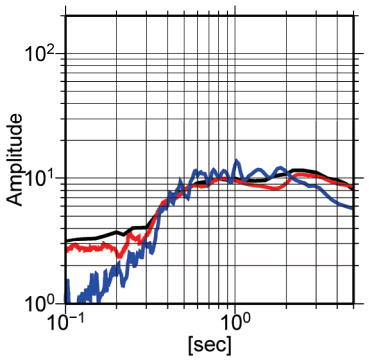

Figure 16. Site amplification factor from the seismic bedrock, studied by Nozu et al(2006). in the Fujisawa observation point of K-NET (Blue line) and that of the ground model of this research (Red line) The amplification at the sites that adopted the shallow-and-deep ground model in Chiba Prefecture (Black line)

Figure 13 and Table 4 show comparisons between the average and variance of Vs of each geological stratum obtained by analyzing all survey points, and the Vs value of the initial model. Comparison of the average velocity AVS30 using the model (Right of Figure 14) with the result from the initial model (Middle of Figure 14) shows that AVS30 is greater than the initial model, mainly in the loam plateau in the north part of Fujisawa City (North side of the dotted line in the figure), and that AVS30 is generally 10-30% lower in the geomorphologic classification (South side of the dotted line in the figure). These results differ from those for AVS30 in the geomorphologic classification (Left of the figure 14) and differ greatly from the results and velocity structure obtained to date. At the same time, if the initial model was compensated by gravity, AVS30 became slightly smaller in the location where the buried valley supposedly existed. However, the results showed good agreement with the period characteristics of the microtremor observation, and the variance of the cycle characteristics between the H/V spectral ratio and the theoretical spectral ratio became smaller in the finial model (Figure 15). The calculated results of the current soil-structure model generally agreed well with the spectral amplification ratio (SH) and the spectral amplification ratio reported by Nozu et al.(2005), which they calculated using the seismic waveform at K-NET Fujisawa observation point (Figure 16).

4. CONCLUSIONS

In this study, the tuning about the geological model created in detail by the gravity observation result for Fujisawa and the foundation structural model using a microtremor observation result was considered. As a result, the foundation structural model which can mainly explain the excellence cycle of the range for 2.0 to 0.2 second was able to be created. In response to this result, examination and verification of the creation technique of optimal sallow and deep integrated structure models for earthquake motion prediction are due to be performed in a wide area from now on.

AKCNOWLEDGEMENT

We express our sincere gratitude to Shohei Naito, Ken Xiansheng Hao, Nobuyuki Morikawa, and Shinichi Kawai of National Research Institute for Science and Disaster Prevention (NIED) for their support during the field survey. We used earthquake and ground data from K-NET of NIED.

REFERENCES

Arai, H. and Tokimatsu, K.(2004). S-Wave Velocity Profiling by Inversion of Microtremor H/V Spectrum, Bulletin of the Seismological Society of America, Vol. 94, No. 1, pp. 53–63.

Matsuoka, M., Wakamatsu, K., Fujimoto, K., and Midorikawa, S. (2005). Estimation of Average Ground S-Wave Velocity using Japan Geology and Ground Classification Map, Collection of papers of Japan Society of Civil Engineers, No. 794/I-72, pp. 239-251.

Fujisawa City Education and Culture Center. (1987). Exploring the Underground of Fujisawa, Collection of borehole logs.

Survey Committee of Estimated Earthquake Damage of Kanagawa Prefecture. (2009). Report on estimated earthquake damage of Kanagawa Prefecture.

Fujiwara, H., Kawai, S., Aoi, S., Morikawa, N., Senna, S., Kudo, N., Ooi, M., Hao, K., Hayakawa, Y., Tohyama, N., Matsuyama, H., Iwamoto, K., Suzuki, H., and Liu, Y. (2009). Review of the Approach to Construct a Nationwide Deep Soil Structure Model for the Evaluation of Strong Earthquakes, Research Material of National Research Institute for Earth Science and Disaster Prevention, 337.

Miyake, H., Kouketsu, K., Furumura, T., Inagaki, Y., Masuda, T., and Midorikawa, S. (2006). Construction of a Shallow Soil Structure for the Prediction of Strong Earthquakes in the Tokyo Metropolitan Area, Collection of papers of the 12th Symposium of Earthquake Engineering in Japan, pp.214–217.

Hiratsuka City Museum. (2007). Ground and Active Faults around Hiratsuka (with attached soil map around Hiratsuka), Handbook of the Special Summer Exhibition, pp. 49.

Nozu, A. and Nagao, T. (2005). Characteristics of Site Amplification in Ports Nationwide based on Spectrum Inversion, material of Port and Airport Research Institute, 1112, pp.56.

Yamanaka, H., Ohori, H. and Midorikawa, S. (2010). Estimation of the Structure of Seamless S-wave Velocity in the Kanto Plain by the Inverse Analysis of Soil Amplifying Characteristics based on Earthquake Records, Architectural Institute of Japan.